Journal of Power Sources 196 (2011) 5623–5630

Contents lists available at ScienceDirect

Journal of Power Sources

journal homepage: www.elsevier.com/locate/jpowsour

V_2O_3 modified $LiFePO_4$/C composite with improved electrochemical performance

Y. Jin [a], C.P. Yang [a], X.H. Rui [a], T. Cheng [b], C.H. Chen [a,*]

[a] CAS Key Laboratory of Materials for Energy Conversion, Department of Materials Science and Engineering, University of Science and Technology of China, 96 Jinzhai Road, Anhui, Hefei 230026, China
[b] Nanjing University of Science and Technology, Jiangsu, Nanjing 210094, China

ARTICLE INFO

Article history:
Received 3 December 2010
Received in revised form 16 February 2011
Accepted 17 February 2011
Available online 26 February 2011

Keywords:
Lithium iron phosphate
Vanadium oxide
Lithium ion battery
Cathode
Diffusion coefficient

ABSTRACT

In addition to lattice doping and carbon-coating, surface modification with other metal oxides can also improve the electrochemical performance of $LiFePO_4$ powders. In this work, highly conductive vanadium oxide (V_2O_3) is in situ produced during the synthesis of carbon-coated $LiFePO_4$ ($LiFePO_4$/C) powders by a solid state reaction process and acts as a surface modifier. The structures and compositions of $LiFePO_4$/C samples containing 0–10 mol% vanadium are analyzed by X-ray diffraction, Raman spectroscopy, scanning electron microscopy and transmission electron microscopy. Their electrochemical properties are also characterized with galvanostatic cell cycling and cyclic voltammetry. It is found that vanadium is present in the form of V_2O_3 that is incorporated in the carbon phase. The vanadium-modified $LiFePO_4$/C samples show improved rate capability and low-temperature performance. Their apparent lithium diffusion coefficient is in the range of 10^{-12} to 10^{-10} $cm^2\ s^{-1}$ depending on the vanadium content. Among the investigated samples, the one with 5 mol% vanadium exhibits the best electrochemical performance.

1. Introduction

With the ongoing depletion of fossil energy resources and global warming, it is necessary to develop large-scale lithium-ion batteries (LIB) for high power applications such as hybrid electric vehicles and energy storage devices. Since the appearance of the first commercial LIB in 1990, cathode materials have always been the most important components of the cells because they generally determine the capacity and safety of LIB. Among the available cathode materials, the iron-based orthophosphate $LiFePO_4$ is believed to be the most probable candidate to be used in the next generation LIB for its high safety, non-toxicity and excellent cycle life [1–4]. However, like most of other phosphates, its intrinsically low electronic conductivity is an adversity that needs to overcome through various structural modifications [5,6]. The strategies to improve the properties of $LiFePO_4$ include the synthesis of nanocrystalline particles [4,7–12], ion doping [15–21], carbon coating [13,14], and non-carbon second phase modification [22].

In this study, we attempt to introduce a metal oxide with high electronic conductivity as the third phase to modify carbon-coated $LiFePO_4$ ($LiFePO_4$/C) particles in order to enhance their conductivity. In literature, some vanadium oxides have been extensively reported to be used as active electrode materials for LIB [23–25]. Also, V_2O_3 possesses a very high electronic conductivity of over 10^3 S cm^{-1} at room temperature [26,27]. Therefore, it is interesting to investigate the influence of V_2O_3 modification on the electrochemical performance of $LiFePO_4$/C composite.

2. Experimental

A solid state reaction method was employed to prepare V_2O_3 modified $LiFePO_4$/C powders. Lithium carbonate (Li_2CO_3, A.R., China Lithium, Shanghai), ferrous oxalate hydrate ($FeC_2O_4{\cdot}2H_2O$, A.R., Asialon, Hefei), ammonium phosphate ($NH_4H_2PO_4$, C.R., China Medicine Group, Shanghai) and ammonium metavanadate (NH_4VO_4, A.R., China Medicine Group, Shanghai) with Li:Fe:P:V molar ratios of $1:1:1:x$ ($x = 0, 0.01, 0.03, 0.05, 0.1$) were mixed in acetone for 6 h through a wet ball-milling process. Then, the mixtures were dried at room temperature in air and subsequently calcined at 330 °C for 10 h under pure nitrogen to obtain five intermediate powders. For the vanadium-free powder ($x = 0$), it was mixed with 7, 10 and 15 wt% glucose and grinded in an agate mortar in order to prepare three solely carbon-coated $LiFePO_4$ powders with different carbon contents. For the other four intermediate powders, they were similarly mixed with 10 wt% glucose. Finally, all of them were sintered at 700 °C for 8 h under nitrogen to obtain seven products including three vanadium-free $LiFePO_4$/C powders (referred as G7, G10 and G15 for the samples prepared with 7, 10 and 15 wt% glucose additive, respectively) and four vanadium-containing LiFePO4/C powders (referred as A, B, C and D for the

* Corresponding author. Tel.: +86 551 3606971; fax: +86 5513601592.
E-mail address: cchchen@ustc.edu.cn (C.H. Chen).

0378-7753/$ – see front matter © 2011 Elsevier B.V. All rights reserved.
doi:10.1016/j.jpowsour.2011.02.059

Table 1
Lattice parameters of the samples calculated from the XRD patterns. For comparison, the standard data and results from Goodenough's work [1] are also listed in the table.

	a (Å)	b (Å)	c (Å)	Volume (Å^3)
PDF-40-1499	6.018	10.340	4.703	292.95
Goodenough's [1]	6.008	10.334	4.693	291.39
Sample A	5.999	10.338	4.695	291.36
Sample B	5.986	10.335	4.706	291.32
Sample C	5.998	10.332	4.702	291.38
Sample D	6.003	10.334	4.694	291.35

samples containing 1, 3, 5 and 10 mol% V, respectively).The structures of the powders were analyzed by X-ray diffraction (XRD, Rigaku TTR-III, CuKα radiation) and Raman spectroscopy (LABRAM-HR). The particle morphology of the powders was observed with a scanning electron microscope (SEM, JSM-6390LA) and a transmission electron microscope (TEM, JEOL-2010).

For electrochemical measurements, the obtained V-modified $LiFePO_4$/C powders (90 wt%) were mixed with acetylene black (5 wt%) and poly(vinylidene fluoride) (Kynar HSV900) binder (5 wt%) in N-methylpyrrolidone to obtain slurries. Each of these slurries was cast onto an aluminum foil to form an electrode laminate. After vacuum drying at 80 °C, the laminates were punched into round discs (1.4 cm in diameter) to be used as the working electrodes of Li/$LiFePO_4$ half-cells. The electrolyte was a solution of 1 M $LiPF_6$ dissolved in ethylene carbonate/diethyl carbonate (1:1, w/w). CR2032 coin-type cells were assembled in an argon-filled glove-box (MBraun Lab Master130).

These cells were cycled on a multi-channel battery cycler (Neware BTS-610, Shenzhen) in the voltage range from 2.2 to 4.0 V during the first 3 cycles at room temperature. The charge mode was a constant current–constant voltage (CC–CV) condition, i.e., the cells were first charged at a constant current of 0.1 mA–4.0 V and then continuously charged at 4.0 V till the current dropped below 0.02 mA. To measure the electrochemical performance at various temperatures, the cells were cycled at 1, 2, 5 C rates at room temperature and at 0.2 C rate at −10 °C in the same voltage range. Note that 1 C rate was equivalent to a current density of 150 mA g^{-1}. Also, the lithium-ion diffusion coefficient (D_{Li^+}) in the electrodes was measured by means of cyclic voltammetry (CV). The CV was performed on a CHI604B electrochemical workstation from 2.0 to 4.0 V at scan rates of 0.05, 0.1, 0.2 and 0.5 mV s^{-1}, respectively.

3. Results and discussion

3.1. Structural analyses

Fig. 1 shows the X-ray diffraction patterns of the V-modified $LiFePO_4$/C powders. Obviously, the main phase in these samples is orthorhombic $LiFePO_4$ with a space group of Pmnb. In addition to the peaks of $LiFePO_4$, the main diffraction peaks (0 1 2), (1 0 4) and (1 1 6) of V_2O_3 are also clearly detected in samples C and D. The formation of V_2O_3 must be resulted from the decomposition of NH_4VO_4 and the carbothermal reduction from V^{5+} to V^{3+}. Based on the amount of NH_4VO_4 in the starting compositions, the theoretical content of V_2O_3 in each final sample is calculated to be 0 wt% (G10), 0.45 wt% (A), 1.4 wt% (B), 2.3 wt% (C) and 4.6 wt% (D), respectively. Because the sensitivity of the XRD analysis is about 2 wt%, V_2O_3 is likely present in samples A and B. Thus, V_2O_3 exists as a second phase instead of lattice doping in all of the V-modified samples. It should be noted that other possible impurity phases like $Li_3V_2(PO_4)_3$, V_2O_5 and FeP_2 are not detected in these samples. Based on this result, we may reasonably presume that the production of $LiFePO_4$ is preferential to that of $Li_3V_2(PO_4)_3$.

Table 1 gives the lattice parameters of the samples calculated from the XRD patterns. For comparison, the standard data and results from Goodenough's work [1] are also listed in the table. The obtained parameters of our four samples are very close to the results of Goodenough et al. This result suggests again that vanadium does not enter the olivine lattice structure and exists as another phase in the V-modified $LiFePO_4$/C composites.

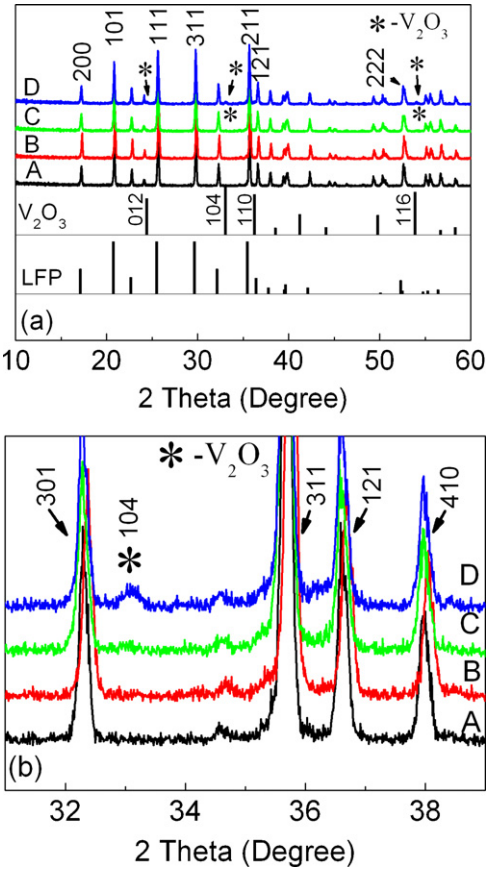

Fig. 1. XRD patterns of four V_2O_3-modified $LiFePO_4$ powders. The standard patterns for $LiFePO_4$ and V_2O_3 are also plotted in the figure.

Raman spectroscopy is employed to investigate the structure of the carbon phase which is amorphous and not detected by XRD. Fig. 2a–c are the Raman spectra of the samples G10 (0 mol% V) (pristine), A (1 mol% V) and C (5 mol% V), respectively. Each of the spectra consists of two intense broad peaks at 1350 and 1600 cm^{-1}. According to Doeff et al. [28,29], these two peaks, namely D-band and G-band, are attributed to carbon and can be fitted with four separated dotted-line peaks at 1194 (peak 1), 1347 (peak 2), 1510 (peak 3) and 1585 cm^{-1} (peak 4), respectively. The peak 2 and peak 4 are contributed by sp^2-type graphite-like structure (i.e., sp^2 C–C bonds), while peak 1 and peak 3 by sp^3-type diamond-like structure (i.e., sp^3 C–C bonds), which is often related to amorphous carbon. Hence the integrated intensity ratio I_{sp^2}/I_{sp^3} can be used to characterize the degree of graphitization of carbon, where I_{sp^2} and I_{sp^3} are the total areas of (peak 2 + peak 4) and (peak 1 + peak 3), respectively. The ratio of I_{sp^2}/I_{sp^3} as a function of vanadium content is plotted in Fig. 2d. The I_{sp^2}/I_{sp^3} values of pristine (0 mol% V), sample A (1 mol% V) and sample C (5 mol% V) are 1.01, 1.04 and 1.35, respectively. Therefore, the degree of graphitization for the carbon in the $LiFePO_4$/C composites increases with the content of vanadium. Because the electron conduction in the $LiFePO_4$/C samples is preferably through the more conductive graphite-like carbon compared to the less conductive amorphous carbon, the conductivity of the $LiFePO_4$/C samples increases accordingly with increasing the vanadium content. In fact, it has been found [30] that some transition metal oxides can improve the graphitization

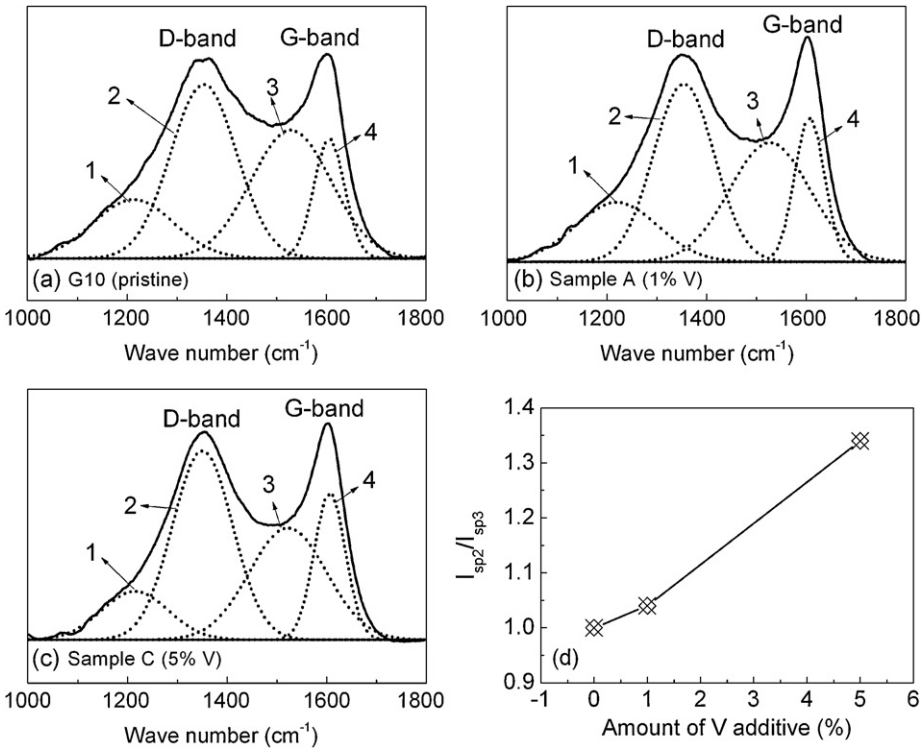

Fig. 2. Raman spectra of (a) pristine, (b) sample A and (c) sample C (the dotted lines are from a Guassian numerical simulation), and (d) the relationship of I_{sp^2}/I_{sp^3} vs. V content.

of carbon decomposed from organics at a relatively low temperature (e.g., 1000 °C). Thus, the improvement of graphitization in our experiment can be attributed to the presence of vanadium oxides.

Fig. 3 shows the SEM images of the V-modified $LiFePO_4$/C samples. It can be seen that the average size of $LiFePO_4$ particles apparently increases with increasing the content of vanadium (from Fig. 3a–d). Considering the high melting point of V_2O_3 (about 2000 °C) and V_2O_5 (670 °C), there is no possibility of liquid sintering process during the synthesis that can cause grain growth. Hence, the difference in particle size is likely caused by the difference in carbon content. The presence of carbon in the composites can restrain the growth of $LiFePO_4$ particles effectively during heat treatment. Because the carbon decomposed from glucose may be partly consumed to reduce V^{5+} into V^{3+}, it is easy to understand that the carbon content decreases with increasing the content of vanadium and consequently the $LiFePO_4$ particles grow larger. The carbon contents in these samples can be determined through an acid-dissolution method, and the results are shown in Fig. 4. It is indeed confirmed that the carbon content drops from about 2.5 wt% (sample A) to 0.9 wt% (sample D). The analysis of element distribution mapping by Energy Dispersive Spectroscopy (EDS) (Fig. 3e and f) displays rather uniform distribution of Fe and V in these samples, indicating that vanadium is everywhere on the grain surface. This result can help us to understand that so small amount of vanadium additive can lead to so remarkable improvement in the electrochemical performance (see below). Table 2 gives the quantity and ratios of elements Fe, P and V in the pristine sample, samples A, B, C and D measured by EDS. Obviously, the atomic ratios among these three elements are quite consistent with the initial composition.

To further determine the existence and location of V_2O_3 in the V-modified $LiFePO_4$/C powders, sample C was analyzed by TEM (Fig. 5). Fig. 5a indicates clearly that a layer of loose carbon coating on the surface of secondary particles of $LiFePO_4$ and fills the interspaces between primary particles of $LiFePO_4$. The diameter of a $LiFePO_4$ grain is approximately 500 nm, being consistent with the result of the SEM analysis (Fig. 3c). If we magnify the selected square area in Fig. 5a and observe the structure of the carbon layer more carefully, many inhomogeneously distributed dark grains are observed to be incorporated in this carbon layer (Fig. 5b). The dark grains have a well-crystallized structure with a diameter of 20 nm that is surrounded by a partially crystallized structure. In the well-crystallized area, the gap between every two parallel stripes is measured to be 0.26 nm, which corresponds to the interplanar spacing distance of (1 0 4) planes of V_2O_3 crystals. Meanwhile, the interplanar spacing distance of the stripes in the light area sur-

Table 2
Quantity and ratios of P, Fe, V elements in samples G10 (i.e., pristine), A, B, C and D measured by EDS.

Element	Atom (%)	Error (%)	Normalization (Fe as 1.00)
Pristine			
P	10.37	0.08	0.97
Fe	10.74	0.12	1.00
V	0	Null	0
Sample A			
P	9.41	0.13	0.95
Fe	9.86	0.38	1.00
V	0.15	0.35	0.02
Sample B			
P	12.36	0.18	0.98
Fe	12.60	0.31	1.00
V	0.35	0.15	0.03
Sample C			
P	8.47	0.11	0.98
Fe	8.61	0.29	1.00
V	0.34	0.20	0.04
Sample D			
P	0.90	0.11	0.99
Fe	10.03	0.29	1.00
V	1.25	0.21	0.12

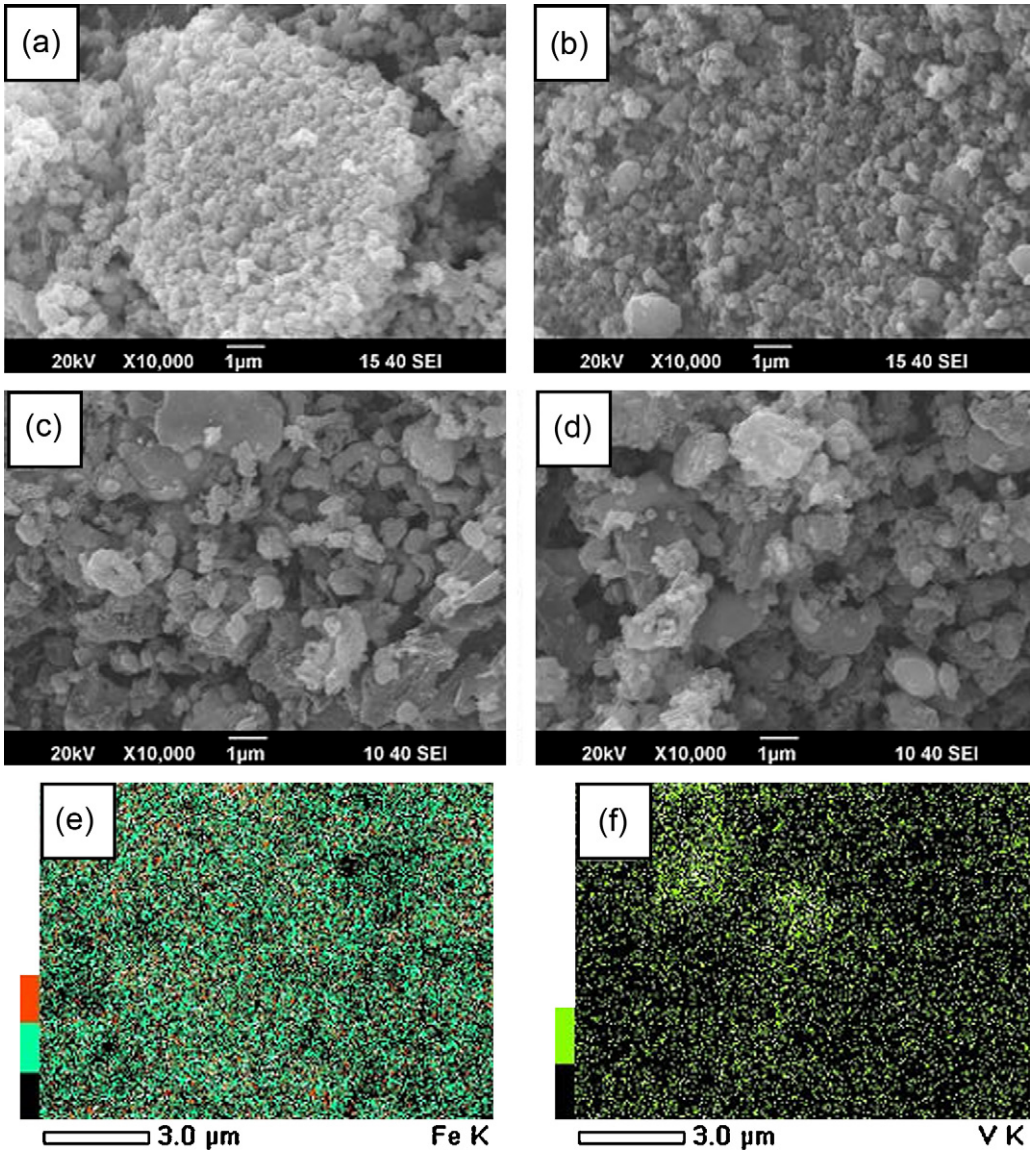

Fig. 3. SEM photos of (a) sample A, (b) sample B, (c) sample C, and (d) sample D. (e) and (f) are the element distribution mappings of Fe and V in sample C by EDS.

rounding V_2O_3 grains is measured to be 0.34 nm, corresponding to the interplanar spacing distance of (1 1 1) planes of graphite. Hence, the surface of $LiFePO_4$ particles is actually modified by a partly graphitized carbon layer that is incorporated with V_2O_3 grains.

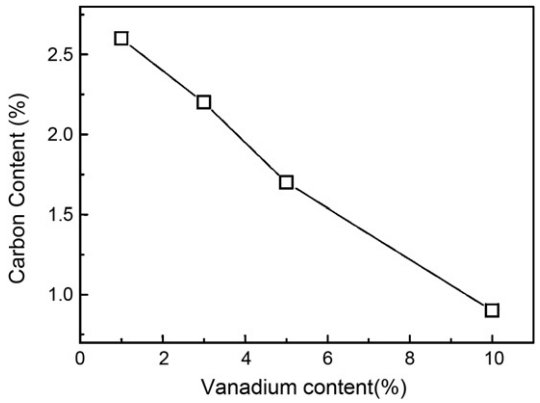

Fig. 4. Relationship of carbon content vs. vanadium content.

3.2. Electrochemical performance

Fig. 6 illustrates the voltage profiles of the half cells with the surface-modified $LiFePO_4$ laminates as the positive electrodes. For the vanadium-free carbon-coated $LiFePO_4$ with different carbon contents (Fig. 6a), the sample prepared with 7 wt% glucose additive has a rather low specific capacity (114 mAh g^{-1}) and a relatively low discharge potential. The samples prepared with 10 and 15 wt% glucose additive have a higher specific capacity of 121 and 122 mAh g^{-1}, respectively. Thus, under the synthesis conditions in this study, the maximal capacity of the carbon-coated $LiFePO_4$ is about 120 mAh g^{-1} and the sample prepared with 10 wt% glucose additive is selected as the baseline and pristine composition for vanadium modification.

It can be seen that during the cycling at room temperature (Fig. 6b), the four V-modified samples give rise to typical voltage profiles of $LiFePO_4$ with very smooth plateaus at 3.46 V (charge) and 3.37 V (discharge) as well as rather vertical tails. The difference between the charge and discharge plateaus is as low as 100 mV, indicating that the polarization of the V-modified samples is low due likely to their good conductivity. On the contrary, the pristine $LiFePO_4$ sample shows a high polarization which leads

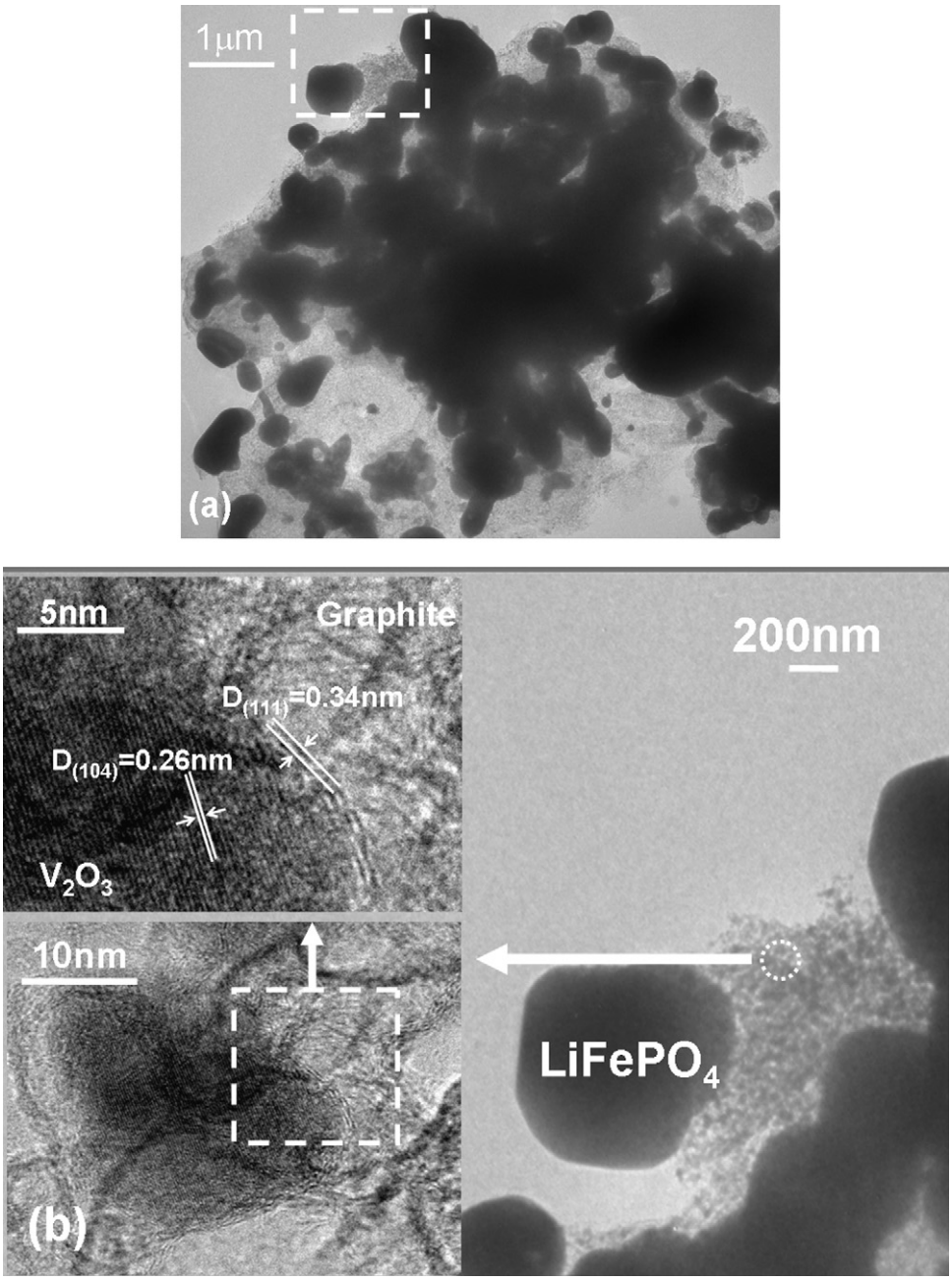

Fig. 5. TEM photo of sample C (a) and the magnified image of the selected area (b).

to a largely divided charge/discharge plateaus and a curved discharge tail. The initial discharge capacity of the five samples is 120.6 mAh g^{-1} (pristine), 132.7 mAh g^{-1} (sample A), 130.4 mAh g^{-1} (sample B), 143.5 mAh g^{-1} (sample C) and 125.5 mAh g^{-1} (sample D), respectively. Among them, the pristine $LiFePO_4$ has the least capacity, suggesting that 10 wt% of glucose additive does not lead to sufficient conductivity [14]. According to the result in Fig. 6a, the enhancement in conductivity cannot be achieved by adding more glucose during the synthesis. Samples A and B show higher capacity due to the positive contribution of vanadium additive. However, compared with sample C containing 5 mol% vanadium, 1 or 3 mol% vanadium additive is not enough to increase the capacity to above 140 mAh g^{-1}. It is evident that the optimal content of vanadium additive is 5 mol% that leads to an initial specific capacity of 143.5 mAh g^{-1} that is over 83% of theoretical capacity (172 mAh g^{-1}) at 0.2 C rate. Since V_2O_3 is an electrochemically inert component in this voltage range [24], the capacity will decrease when the amount of vanadium additive is too much, which is the case for sample D containing 10 mol% vanadium.

Fig. 6c shows the voltage profiles of these cells at a low temperature of −10 °C. Compared with the room temperature performance, the voltage profiles vary a lot. Among the five samples, sample C also exhibits the best performance in capacity (about 135 mAh g^{-1}) and the least polarization. Meanwhile, the pristine sample shows a rather poor performance with a low capacity of less than 60 mAh g^{-1} and a large polarization.

Fig. 7 shows the cycling behaviors of the five samples at room temperature. The four V-modified samples reveal higher capacity than the pristine sample, especially when the current is above 1 C rate. From 0.2 to 2 C rate, the capacity and cycling performance of the four V-modified samples cannot be distinguished very easily. But, on a severe condition of long life cycling at 5 C rate, their capac-

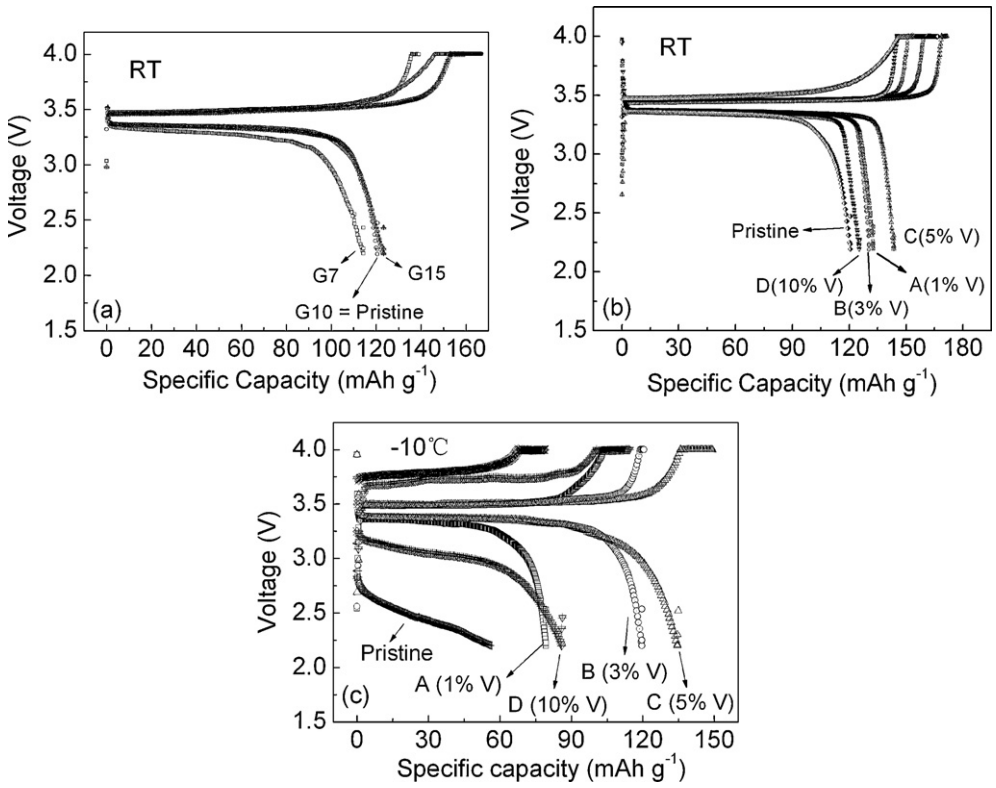

Fig. 6. Voltage profiles of samples G7, G10 (i.e., pristine) and G15 (a). The pristine sample, samples A, B, C and D at room temperature (b) and −10 °C (c). The current rate was 0.2 C.

ities vary remarkably and a sufficient vanadium (above 5 mol%) can significantly suppress the reduction in capacity with current rising. When the vanadium additive amount is 5 mol% (sample C), the capacity can remain at a high value of over 100 mAh g^{-1} at 5 C rate even after 50 cycles. Sample B also shows an evident rise in capacity compared with the pristine sample or sample A with less amount of vanadium. Considering the relatively large primary particles in samples C and D (Fig. 3), it is reasonable that their high C-rate capacity is lower than Dahn's result [14].

3.3. Apparent lithium ion diffusion coefficient

Cyclic voltammetry (CV) measurement at different scan rates can be used to derive the lithium ion diffusion coefficient in an electrode material. However, it is usually valid for an intercalation compound in a single-phase region such as $LiCoO_2$. As for $LiFePO_4$, there are coexistence of two phases, i.e., $LiFePO_4$ and $FePO_4$ during the lithium insertion and extraction. Therefore, the diffusion coefficient thus derived has only apparent meaning. A number of groups have adopted this approach for similar two-phase-coexisting electrode materials such as $Li_3V_2(PO_4)_3$ [31] and $LiFePO_4$ [18,22]. In this study, to make a parallel comparison on the samples with different vanadium contents, their apparent lithium ion diffusion coefficients derived from CV are helpful.

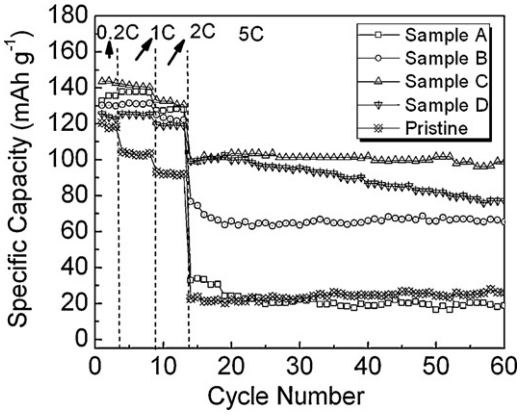

Fig. 7. Cycling behaviors of the pristine sample, samples A, B, C and D at room temperature. The current rate was 0.2–5 C.

Fig. 8a shows the CV curves of sample C at a scan rate from 0.05 to 0.5 mV s^{-1}. It is obvious that the intensity and area of the redox peaks increase with the scan rate. The linear relationship of the peak current (i_p) as a function of square root of scan rate ($v^{1/2}$) is illustrated in Fig. 8b. Thus, the apparent diffusion coefficient can be derived according to following Eq. (1):

$$i_p = (2.69 \times 10^5) n^{3/2} A D_{Li^+}^{1/2} C_{Li}^* v^{1/2} \quad (1)$$

where, i_p is the peak current (A), n is the charge-transfer number (one), A is the contact area between $LiFePO_4$ and electrolyte (here A approximates the surface area of electrode, 1.54 cm^2), C_{Li}^* is the concentration of lithium ions in the cathode (0.023 mol cm^{-3}), and v is the scan rate (V s^{-1}). Based on the slopes of the lines in Fig. 8b, the apparent diffusion coefficients ($D_{Li^+}^{app}$) of samples A, B, C and D are calculated to be 1.5×10^{-11}, 6.1×10^{-11}, 1.3×10^{-10} and 1.7×10^{-11} cm^2 s^{-1}, respectively, during charge, and 8.0×10^{-12}, 3.5×10^{-11}, 7.6×10^{-11} and 6.5×10^{-12} cm^2 s^{-1}, respectively, during discharge. These results are also illustrated in Fig. 8c. The values of the apparent diffusion coefficient vary from 10^{-12} to 10^{-10} cm^2 s^{-1} depending on the amount of vanadium additive. Sample C gives the highest value, being consistent with the electrochemical performance measurements (Figs. 6 and 7). The difference

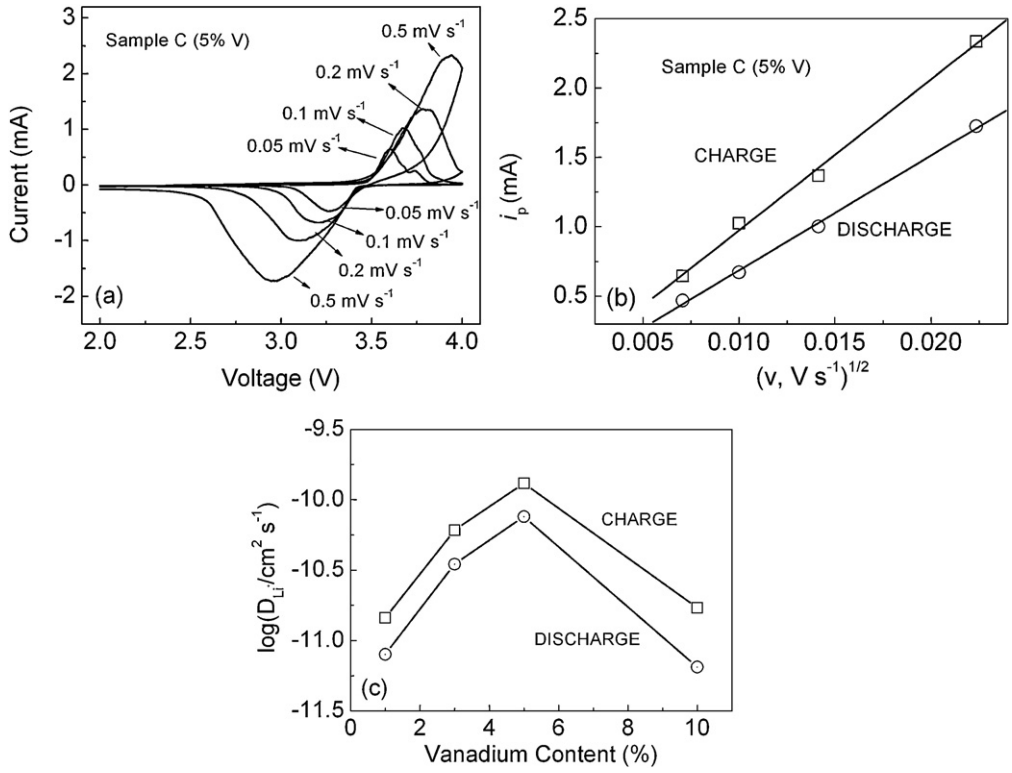

Fig. 8. Cyclic voltammetry of V_2O_3-modified $LiFePO_4$/C electrodes to derive apparent lithium ion diffusion coefficient. (a) Cyclic voltammograms of sample C in the voltage range of 2.0–4.0 V at scan rates of 0.05, 0.1, 0.2 and 0.5 mV s^{-1}. (b) The relationship of peak current (i_p) and the square root of scan rate ($v^{1/2}$). (c) The relationship of $log(D_{Li^+}^{app})$ and vanadium content.

in $D_{Li^+}^{app}$ is the reflection of the difference in the rate of transport for lithium ions in the electrodes. It is collectively determined by three factors: surface resistance, lithium ion diffusion and phase transition ($LiFePO_4$ and $FePO_4$) along the internal boundary diffusion coefficient. As discussed before, sample C has the least surface resistance due to the relatively high degree of graphitization and adequate content of V_2O_3 so that it is reasonable that its $D_{Li^+}^{app}$ is the highest.

4. Conclusions

Through a simple solid state reaction process, V_2O_3 modified $LiFePO_4$/C composite powders have been prepared. The nanoscale V_2O_3 particles are incorporated in the carbon coating structure uniformly and $LiFePO_4$ particles are collectively modified by this carbon–V_2O_3 surface layer. Raman spectroscopy analysis indicates that the V_2O_3 particles can increase the graphitization degree of the carbon coating and consequently the electronic conductivity of the electrodes. The V_2O_3-modified $LiFePO_4$/C materials exhibit improved electrochemical performance both in rate capability and low-temperature behavior. The measurement of the apparent lithium ion diffusion coefficient has proved that the good electronically conducting carbon–V_2O_3 layer can significantly facilitate the lithium ion transport in the $LiFePO_4$/C electrodes.

Acknowledgements

This study was supported by National Science Foundation of China (grant no. 20971117 and 10979049) and Education Department of Anhui Province (grant no. KJ2009A142). We are also grateful to the Solar Energy Operation Plan of Academia Sinica.

References

[1] A.K. Padhi, K.S. Nanjundaswamy, J.B. Goodenough, J. Electrochem. Soc. 144 (1997) 1188.
[2] A.K. Padhi, K.S. Nanjundaswamy, C. Masquelier, S. Okada, J.B. Goodenough, J. Electrochem. Soc. 144 (1997) 1609.
[3] M. Thackeray, Nat. Mater. 1 (2002) 81.
[4] A. Yamada, S.C. Chung, K. Hinokuma, J. Electrochem. Soc. 148 (2001) A224.
[5] H. Huang, S.C. Yin, L.F. Nazar, Electrochem. Solid-State Lett. 4 (2001) A170.
[6] N. Ravet, Y. Chouinard, J.F. Magnan, S. Besner, M. Gauthier, M. Armand, J. Power Sources 97–8 (2001) 503.
[7] C. Delacourt, P. Poizot, S. Levasseur, C. Masquelier, Electrochem. Solid-State Lett. 9 (2006) A352.
[8] F. Croce, A.D. Epifanio, J. Hassoun, A. Deptul, T. Olczac, B. Scrosati, Electrochem. Solid-State Lett. 5 (2002) A47.
[9] Y.Q. Hu, M.M. Doeff, R. Kostecki, R. Finones, J. Electrochem. Soc. 151 (2004) A1279.
[10] K.S. Park, J.T. Son, H.T. Chung, S.J. Kim, C.H. Lee, H.G. Kim, Electrochem. Commun. 5 (2003) 839.
[11] G. Meligrana, C. Gerbaldi, A. Tuel, S. Bodoardo, N. Penazzi, J. Power Sources 160 (2006) 516.
[12] S.F. Yang, P.Y. Zavalij, M.S. Whittingham, Electrochem. Commun. 3 (2001) 505.
[13] P.P. Prosini, D. Zane, M. Pasquali, Electrochim. Acta 46 (2001) 3517.
[14] Z. Chen, J.R. Dahn, J. Electrochem. Soc. 149 (2002) A1184.
[15] A. Yamada, S. Chung, J. Electrochem. Soc. 148 (2001) A960.
[16] D.Y. Wang, H. Li, S.Q. Shi, X.J. Huang, L.Q. Chen, Electrochim. Acta 50 (2005) 2955.
[17] J. Barker, M.Y. Saidi, J.L. Swoyer, Electrochem. Solid-State Lett. 6 (2003) 53.
[18] N. Hua, C.Y. Wang, X.Y. Kang, T. Wumair, Y. Han, J. Alloys Compd. 503 (2010) 204.
[19] J. Hong, C.S. Wang, X. Chen, S. Upreti, M.S. Whittingham, Electrochem. Solid-State Lett. 12 (2009) A33.
[20] H. Liu, Q. Cao, L.J. Fu, C. Li, Y.P. Wu, H.Q. Wu, Electrochem. Commun. 8 (2006) 1553.
[21] S.Y. Chung, J.T. Bloking, Y.M. Chiang, Nat. Mater. 1 (2002) 123.
[22] Y. Liu, C.H. Mi, C.Z. Yuan, X.G. Zhang, J. Electroanal. Chem. 628 (2009) 73.
[23] M. Koltypin, V. Pol, A. Gedanken, D. Aurbach, J. Electrochem. Soc. 154 (2007) A605.
[24] A.M. Cao, J.S. Hu, H.P. Liang, L.J. Wan, Angew. Chem. 117 (2005) 4465.
[25] P.P. Prosini, T. Fujieda, S. Passerini, M. Shikano, T. Sakai, Electrochem. Commun. 2 (2000) 44.

[26] C. Grygiel, A. Pautrat, Phys. Rev. B 79 (2009) 235111.
[27] M.M. Qazilbash, A.A. Schafgans, K.S. Burch, S.J. Yun, B.G. Chae, B.J. Kim, H.T. Kim, D.N. Basov, Phys. Rev. B 77 (2008) 115121.
[28] M.M. Doeff, Y. Hu, F. McLarnon, R. Kostecki, Electrochem. Solid-State Lett. 6 (2003) A207.
[29] Y. Hu, M.M. Doeff, R. Kostecki, R. Finones, J. Electrochem. Soc. 151 (2004) A1279.
[30] M. Inagaki, K. Fujita, Y. Takeuchi, K. Oshida, H. Iwata, H. Konno, Carbon 39 (2001) 921.
[31] X.H. Rui, N. Ding, J. Liu, C. Li, C.H. Chen, Electrochim. Acta 55 (2010) 2384.